Metallomics

Integrated biometal science

Accepted Manuscript

This article can be cited before page numbers have been issued, to do this please use: J. C. Cristaldi, F. M. Ferroni, A. Dure, C. Ramirez, S. Dalosto, A. C. Rizzi, P. Gonzalez, M. G. Rivas and C. D. Brondino, *Metallomics*, 2020, DOI: 10.1039/D0MT00177E.

ROYAL SOCIETY OF CHEMISTRY

rsc.li/metallomics

DOI: 10.1039/D0MT00177E

Heterologous production and functional characterization of *Bradyrhizobium japonicum* copper-containing nitrite reductase and its physiological redox partner cytochrome c_{550}

Julio C. Cristaldi,[a] Felix M. Ferroni,[a] Andrea B. Duré,[a] Cintia S. Ramírez,[a] Sergio D. Dalosto,[b] Alberto C. Rizzi,[a] Pablo J. González,[a] Maria G. Rivas,[a] and Carlos D. Brondino*[a]

[a]Departamento de Física, Facultad de Bioquímica y Ciencias Biológicas, Universidad Nacional del Litoral and CONICET, S3000ZAA Santa Fe, Argentina

[b]Instituto de Física del Litoral, CONICET-UNL, Güemes 3450, S3000GLN Santa Fe, Argentina

*email: brondino@fbcb.unl.edu.ar, Tel: +54-342-457 5213

URL: https://www.fbcb.unl.edu.ar/dfbioq/

Abstract

Two domain copper-nitrite reductases (NirK) contain two types of copper centers, one electron transfer (ET) center of type 1 (T1) and a catalytic site of type 2 (T2). NirK activity is pH-dependent, which has been suggested to be produced by structural modifications at high pH of some catalytically relevant residues. To characterize the pH-dependent kinetic of NirK and the relevance of T1 covalency in intraprotein ET, we studied the biochemical, electrochemical, and spectroscopic properties complemented with QM/MM calculations of *Bradyrhizobium japonicum* NirK (*Bj*NirK) and of its electron donor cytochrome c_{550} (*Bj*CycA). *Bj*NirK presents absorption spectra determined mainly by a S(Cys)3pπ→Cu^{2+} ligand-to-metal charge-transfer (LMCT) transition. The enzyme shows low activity likely due to the higher flexibility of a protein loop associated with *Bj*NirK/*Bj*CycA interaction. Nitrite is reduced at high pH in a T1-decoupled way without T1→T2 ET in which proton delivery for nitrite reduction at T2 is maintained. Our results are analyzed in comparison with previous results found by us in *Sinorhizobium meliloti* NirK, whose main UV-vis absorption features are determined by S(Cys)3pσ/π→Cu^{2+} LMCT transitions.

Significance to metallomics

Rhizobacteria are denitrifiers of great relevance to biofertilization processes. Considerable efforts have been devoted to characterize the reaction mechanism of the transition metal-containing enzymes involved in the denitrifying metabolic pathway of these bacteria. The current investigation is focused on the biochemical characterization of the copper-containing nitrite reductase from *Bradyrhizobium japonicum*, a redox enzyme that catalyzes the one-electron reduction of NO_2^- to NO, and of its physiological electron donor cytochrome c_{550}.

View Article Online
DOI: 10.1039/D0MT00177E

Introduction

Copper-containing nitrite reductases (NirK) catalyze the second step of denitrification process through the one-electron reduction of nitrite (NO_2^-) to nitric oxide (NO) ($E^{o'}$ = +370 mV vs SHE).[1, 2] Best characterized NirK are homotrimers that contain two Cu atoms *per* monomer ~ 12 Å apart, one of type 1 (T1 or blue copper) and the other of type 2 (T2 or normal copper).[3, 4] T1 and T2 are the electron transfer (ET) and the catalytic centers, respectively.[5, 6] T2 is a four coordinate copper site bound to a labile water molecule and three N atoms from histidine imidazoles in a distorted tetrahedral geometry. T1 copper(II) ion is also tetracoordinated with three strong ligands, two N atoms from histidine imidazoles and a cysteine thiolate group, and a weaker methionine thioether group.[7-9] Each subunit of NirK is structurally organized in two domains; more recently NirK having subunit composition with extra domains have been reported. These extra domains contain additional redox cofactors whose nature, iron or copper, depends on the microorganism these enzymes have been identified.[10-14]

NirK are subgrouped into blue, green, and greenish-blue according to the electronic properties of T1.[15, 16] Blue NirK shows a very intense absorption at 600 nm and a little absorption at ~ 450 nm, whereas green NirK show absorbance at ~ 450 nm larger than that at 600 nm. Greenish-blue are in between these two extremes with different A_{450}/A_{600} ratios. The distinctive absorption bands of NirK depend mainly on the interactions between the Cu($3d_{x^2-y^2}$) magnetic orbital and the 3p orbitals of the S(Cys) ligand. The lower-energy absorption at ~ 600 nm results from a S(Cys)-3pπ to Cu-3d ligand-to-metal charge-transfer (LMCT) transition, whereas the higher-energy absorption at ~ 450 nm from S(Cys)-3pσ to Cu-3d LMCT transition.[17, 18] Thus, the relative intensity of the absorption bands in NirK reflects mainly the predominant type of the S(Cys)-Cu interaction.

The proposed reaction mechanism for nitrite reduction catalyzed by NirK implies a one-electron reduction coupled to two protons.[19, 20] The electron required for substrate reduction is provided by small electron carrier proteins like azurin, pseudoazurin or *c*-type cytochromes according to the ET reaction: electron donor→T1→T2→nitrite.[9, 21] Blue NirK utilize as electron donors azurins[22, 23] or cytochromes *c*,[24] while green NirK pseudoazurins.[25-27] T1 and T2 are connected by two main chemical pathways; the shortest one, the Cys-His bridge, is thought to transport the electron for nitrite reduction; the longest pathway, which has been called the substrate-sensing loop, is thought to work as a relay that triggers the T1→T2 electron flow through the Cys-His bridge when nitrite is bound to T2.[8, 16, 21] The Cys-His pathway presents two sub-pathways that can serve as potential ET conduits. One of them is the covalent pathway that involves the protein backbone and the side chains of the Cys and His residues, whereas the other one is a hydrogen bond-mediated pathway involving the His-$N^{\delta 1}$ and the Cys O-carbonyl atoms (hereafter the $N^{\delta 1}H\ldots O{=}C$ H-bond) that partially shortcuts the T1-T2 bridging covalent link. Computational calculations suggested that in blue NirK (π-type T1) ET would occur through the pure covalent pathway, while green NirK (σ-type T1) would perform a more efficient ET through the H-bond shortcut.[28] Thus, it seems that these ET pathways would be selectively activated depending on the electronic structure of T1.

The sensing loop pathway contains an aspartic acid residue (Asp_{CAT}) that forms a H-bond with the T2 labile water molecule in the enzyme resting state and with a nitrite O-atom in the nitrite-reacted NirK. Asp_{CAT} is supposed to sense the binding of nitrite to T2,[29, 30] after which Asp_{CAT} by means of a still unknown mechanism would trigger the delivery of one electron from T1 to T2 through the Cys-His bridge. Asp_{CAT} was found to be conserved in most NirK, but a recent report of the structure of the three-domain NirK from *Thermus scotoductus SA-01* (*Ts*NirK) revealed that it can be substituted by a serine residue.[13] Structural data of *Ts*NirK

View Article Online
DOI: 10.1039/D0MT00177E

shows that the serine side chain hydroxyl group is hydrogen bonded to T2 like Asp_{CAT}, but its $pK_a > 12$ would preclude its involvement in proton transfer. A second essential residue in catalysis is a His residue (His_{CAT}) that is linked to Asp_{CAT} through a hydrogen-bonded bridging water molecule.[29, 31, 32] Asp_{CAT} and His_{CAT} are thought to be involved in the pH dependence of the catalytic activity. However, it has been suggested that His_{CAT} has a more relevant role than Asp_{CAT} in the pH-dependent activity, and that the hydrogen bond network of water molecules in the main proton channel, but not the sensing loop, changes its conformation upon nitrite binding.[33]

Distinct types of factors have been indicated as possible causes for the lack of activity of NirK at high pH. The X-ray structure of *Rhodobacter sphaeroides* 2.4.3 NirK (*Rs*NirK) at pH 8.4 showed that, in contrast to the structure at pH 6.0, the H-bond between Asp_{CAT} and T2 labile water molecule is absent, and that the His_{CAT} imidazole plane is moved towards the T2 copper ion but showing higher disorder. The former led to propose that Asp_{CAT} is deprotonated at high pH, which in conjunction with the latter were considered to be as two possible causes for the lack of activity.[34] Furthermore, EPR-monitored redox titrations of as-prepared *Rs*NirK poised at pH 8.4 determined a T2 reduction potential 81 mV lower than that at pH 6.0. Therefore, despite it was not taken into consideration the well-known fact of the role of nitrite in modulating the reduction potential of T2,[35] it was concluded as an additional factor a less favorable T1→T2 ET.[34] Some of these conclusions, *e.g.* a deprotonated Asp_{CAT} and a very low T2 reduction potential but for a nitrite-T2 complex at high pH which would preclude T1→T2 ET during catalysis, were also proposed from spectroscopic and computational studies.[36] However, the high pH X-ray crystal structure of nitrite-bound *Rs*NirK showed that nitrite is not only bound to T2, but also favorably oriented to interact through H-bond interaction with Asp_{CAT}.[34] These observations suggest that additional factors

View Article Online
DOI: 10.1039/D0MT00177E

such as the nature of the Cys-His bridge and the T1 covalency in ET should be taken into account to explain the pH-dependent kinetic activity of NirK.

The regulation of the *in-vivo* activity of NirK beyond its structural implications is determined by genetic arrangements in operons whose expression is fine-tuned by oxygen and nitrate levels in free living cells.[1] Microaerobic conditions are required for the expression of the genes related to NirK and the corresponding redox partner in rhizobacteria like *Bradyrhizobium japonicum* USDA110 and *Sinorhizobium meliloti* 2011.[37, 38] *S. meliloti* possesses the *nir*K and *azu*1 genes within the same operon located in the pSymA megaplasmid,[39] while in *B. japonicum* both *nir*K and *cyc*A genes, are located in the chromosome but far away from each other.[40] The NirK activity has shown to be highly relevant for plant-bacteria symbiosis as *nir*K-deficient *B. japonicum* USDA110 strain has lower capacity to generate nodules in soya,[41] although it has not shown any change in nitrogen fixation activity. Even though both metabolic pathways compete for electrons, they do not use the same physiological electron donors to catalyze their respective reactions in *B. japonicum* USDA110.[42] As briefly discussed, there is a considerable amount of literature related to genetic and metabolic studies of the denitrification process in *B. japonicum* USDA 110 and rhizobia in general, but studies about the enzymes and electron transfer proteins involved in the denitrifying pathway of these microorganisms are scarce.

We report here the biochemical, electrochemical, and spectroscopic characterization together with QM/MM calculations of the two-domain NirK from *B. japonicum* USDA 110 (*Bj*NirK) and of its electron donor cytochrome c_{550} (*Bj*CycA). pH-dependent studies in which the oxidation states of the copper centers are monitored by UV-vis and EPR at the end of the catalytic reaction are used to gain insight on the T1-T2 ET process in NirK, to learn on the the pH-dependent catalytic activity of *Bj*NirK, and whether the electronic structure of T1 is

crucial to determine the intraprotein ET pathway. These results are analyzed in comparison with studies of the green type NirK from *Sinorhizobium meliloti* (*Sm*) we have previously published[43] and of NirK from other bacteria.

Experimental

Cloning and overexpression of *Bj*NirK and *Bj*CycA

Cell growth and DNA extraction of *B. japonicum* USDA 110 were performed as reported elsewhere.[44] The *Bj nirK* gene (locus tag blr7089) was amplified using two specific oligonucleotides (Fwd: 5'-CATATGCTTCCGATGTTCACCCG-3'; Rev: 5'-GAGCTCCTAGTTGGTGTTGGC-3') which include the *Nde*I and *Sac*I restriction sites. Amplification was performed using *Pfu* DNA polymerase from Genbiotech according to manufacturer's instructions. The *nirK* gene was cloned into pJET2.1 blunt (Thermo Fisher) and subcloned into pET22b(+) vector (Novagen) to obtain p22BK expression constructs.

The *B. japonicum* USDA 110 *cycA* gene (locus tag blr7544, cytochrome c_{550})[40] was amplified using a Fwd primer (5′-CATATGACAAAACTGACTTTCGG-3′) and a Rev primer(5′-GGATCCTTACTGCTTGATCTTCC-3′) including *Nde*I and *Bam*HI restriction sites, respectively. Amplification reaction was performed as indicated for *nirK* gene. Amplicons were cloned into pJET2.1 blunt and subcloned into pET22b(+) vector to obtain p22BC expression construct.

Recombinant plasmid constructions were maintained into *E. coli* TOP10 cells (Invitrogen) at -80 °C. DNA sequences were verified by using the Sanger method.[45]

Protein heterologous production and purification

Overexpression of the *nirK* gene from *B. japonicum* USDA 110 was achieved by introducing p22BK into *E. coli* BL21 (DE3) (New England Biolabs Inc.). The transformed strain was grown aerobically at 37 °C overnight with agitation at 200 rpm in Lysogeny broth with 100 μg mL^{-1} ampicillin as starter culture. Protein production was performed using 400 mL (1/100 starter culture) of auto-induction media (ZYP50502)[46] plus 100 μg mL^{-1} ampicillin without lactose and maintained at 37 °C for 24 h (200 rpm). Then, 200 mM $CuSO_4$ was added and maintained in the same condition for 1 h. Finally, protein expression was induced with 250 μM Isopropyl-β-D-1-thiogalactopyranoside (IPTG) at 20 °C and 50 rpm for 3 h. Cells were harvested through centrifugation (4000 × *g* for 20 min) and re-suspended in 20 mM Tris-HCl buffer pH 8.0. The cell suspension (0.1 g wet weight mL^{-1}) was disrupted by sonication. The soluble extract was recovered by centrifugation at 25000 × *g* for 1 h and dialyzed overnight against 20 mM Tris–HCl buffer pH 8.0 supplemented with 100 mM $CuSO_4$ and then centrifuged at 25000 × *g* for 1 h. *Bj*NirK from the soluble extract was purified in three chromatographic steps. The soluble extract was applied to an anion exchange column (DEAE Sepharose Fast Flow, 180 mL, GE Healthcare) equilibrated in 20 mM Tris–HCl buffer pH 8.0 and eluted with a 0–500 mM linear gradient of NaCl in 3.5 column volumes. Deep blue fractions containing *Bj*NirK were pooled and dialyzed against 20 mM Tris–HCl buffer pH 8.0 plus 100 mM $CuSO_4$. The dialyzed pool was loaded onto a Source 15Q column (26 mL, GE Healthcare) equilibrated with 20 mM Tris–HCl buffer pH 8.0. Bound proteins were eluted applying a 0 to 600 mM NaCl linear gradient in 7.6 column volumes. Finally, fractions with *Bj*NirK were concentrated using an Amicon Ultra 30 K NMWL device and loaded onto a Superdex S200 column (74 mL, GE Healthcare) equilibrated with 20 mM Tris–HCl buffer pH 8.0 plus 200 mM NaCl. 500 μL fractions were loaded and eluted isocratically. *Bj*NirK

fractions were pooled and concentrated to approximately 20 mg mL^{-1} in 20 mM Tris–HCl buffer pH 8.0 and stored at −80 °C until use.

Overexpression of the *cycA* gene from *B. japonicum* USDA 110 was achieved by introducing p22BC into *E. coli* BL21 (DE3) Gold (Agilent Technologies) previously transformed with the pEC86 plasmid [47]. The transformed strain was grown aerobically at 37 °C overnight with agitation at 200 rpm in Lysogeny broth containing 100 μg mL^{-1} ampicillin and 34 μg mL^{-1} chloramphenicol as starter culture. Protein production was performed using 400 mL (1/100 starter culture) of auto-induction media (ZYP50502)[46] plus 100 μg mL^{-1} ampicillin, 34 μg mL^{-1} chloramphenicol, and 6 μM hemin and maintained at 20 °C for 48 h (200 rpm). Intense red cells were harvested through centrifugation (4000 × *g* for 20 min) and re-suspended in 20 mM Tris-HCl buffer pH 8.0. After cell disruption and centrifugation, the soluble extract was dialyzed overnight against 5 mM potassium phosphate buffer pH 6.0 and loaded onto a cationic exchange column (SP sepharose fast flow, GE Healthcare, 30 mL) equilibrated with the same buffer and eluted with a 0–500 mM linear gradient of NaCl in 10 column volumes. Faint pink fractions were pooled, concentrated, and injected on a Superdex S200 column (GE Healthcare, 47 mL) equilibrated with 50 mM potassium phosphate buffer pH 6.0 plus 150 mM NaCl. *Bj*CycA fractions were pooled and concentrated to approximately 20 mg mL^{-1} in 20 mM Tris–HCl buffer pH 8.0 and stored at −80 °C until use.

*Bj*NirK and *Bj*CycA purity was evaluated by SDS-PAGE and followed by UV-vis spectroscopy along the purification procedure.

Protein quantification, molecular mass determination, and copper content

Protein concentration was determined using the Lowry method using bovine serum albumin as standard.[48]

Copper content of as-purified nitrite reductase was determined by atomic absorption spectrometry (Perkin Elmer PinAAcle 900T).

Molecular masses of as-isolated proteins were estimated by gel filtration chromatography monitored by a FPLC device (Akta Basic, GE Healthcare) using Superdex 200 and Superdex 75 HR 10/30 columns, GE Healthcare, for *Bj*NirK and *Bj*CycA, respectively. Superdex 200 and 75 columns were equilibrated with 50 mM sodium phosphate buffer pH 7.0 plus 150 mM NaCl, and 10 mM Tris-HCl pH 8.0 buffer plus 200 mM NaCl, respectively. Ferritin (440 kDa), aldolase (158 kDa), conalbumin (75 kDa), carbonic anhydrase (30 kDa), and ribonuclease A (13.7 kDa) were used as standards for the Superdex 200 column, whereas aprotinin (6.5 kDa), ribonuclease (13.7 kDa), carbonic anhidrase (29 kDa), ovalbumin (44 kDa) and conalbumin (75 kDa) for the Superdex 75 column. Isocratic elution was performed at a flow rate of 0.4 mL min^{-1} with detection at 280 nm. The molecular mass of the subunits was estimated by SDS-PAGE according to the method of Laemmli.[49] Samples were treated with sample buffer for 5 min at 100 °C and then loaded onto 15 % and 12 % denaturing polyacrylamide gel for *Bj*CycA and *Bj*NirK, respectively. Mid-range protein molecular weight standards from Genbiotech were used.

Activity assays

Kinetic assays using the artificial electron donor methyl viologen (MV) were performed using a discontinuous method as previously reported.[43] Solutions containing variable concentrations of sodium nitrite (0-4 mM range) and reduced methyl viologen (1.4 mM plus 100 mM sodium dithionite) were mixed to a final volume of 200 µL. All solutions were prepared in a buffer containing MES, CAPS, and Tris-HCl pH 6 (30 mM each). The kinetic reaction was started by adding 50 µL of 250 nM protein and incubated for 2.5 min at 25 °C. To stop the reaction, 25 µL of each mixture was added to the buffer solution (final volume

250 µL) and immediately vigorously stirred. The solution was reacted with 250 µL of sulfanilamide (1 % in 3 M HCl) and 250 µL of N-(1-naphtyl)ethylendiamine (10 % in buffer) for 10 min, after which a pink color was developed. Absorbance was recorded at 540 nm. The consumed nitrite was determined by comparing the absorbance against a reaction blank without enzyme.

Enzyme kinetic studies using the physiological electron donor (*Bj*CycA) were performed by chronoamperometry as described below under electrochemistry methods.

UV–vis mediated redox titrations

Redox titration of *Bj*NirK (65 µM protein in 100 mM potassium phosphate buffer pH 7.0) was performed under anaerobic conditions at 20 °C as described elsewhere recording absorption spectra at each equilibrium potential.[50] Dithionite was used as the reducing agent for titrations, and the mediators dyes (30 nM each) were methyl viologen (−440 mV), neutral red (−325 mV), anthraquinone (−225 mV), phenazine (−125 mV), indigo tetrasulfonic acid (−46 mV), duroquinone (5 mV), galocyanine (30 mV), phenazine etasulfate (55 mV), phenazine metasulfate (80 mV), 2,5-dimethyl benzoquinone (180 mV), and 2,6-dichlorophenol indophenol (217 mV). UV-vis absorption spectra were collected using a diode array spectrophotometer (Cary Agilent 8454). The solution potential were measured using platinum as measuring electrode, and a saturated Ag/AgCl reference electrode calibrated with saturated quinhydrone solution at pH 7.0 and pH 4.0 at room temperature. All the potentials are referred to the standard hydrogen electrode (SHE).

Electrochemistry methods

Cyclic voltammetry (CV) and chronoamperometry were performed on a Teq_4 potentiostat/galvanostat (NanoTeq) and data were analyzed using the Teq_4 software package and Microcal Origin (OriginLab Corp.). A conventional three-electrode

electrochemistry cell was used, with a 3 mm diameter polycrystalline gold disk electrode (BASi), a platinum electrode and a saturated Ag/AgCl electrode as working, auxiliary and reference electrodes, respectively. Sample setup was performed as described previously but using 500 mM glycine as stabilizer in the electrolyte solution.[43, 51] The gold electrode was successively polished with 1, 0.3, and 0.05 μm water alumina slurry (Buehler) and then sonicated in ultrapure water. The polished electrode was subsequently immersed in 1 mM 4,4'-dithiodipyridine solution for 10 minutes. Then, 4 μL of 1 mg/mL *Bj*CycA solution, or *Bj*NirK+ *Bj*CycA (1 mg/mL each) was deposited on the electrode, incubated for 5 minutes, and a square piece of dialysis membrane (3,500-Da cutoff) was placed on the top of the electrode and fitted with an O-ring. The electrode was then placed in a buffered electrolytic solution of pH 6 containing MES, CAPS, and Tris-HCl (30 mM each), 0.1 mM NaCl, and 500 mM glycine. The solution was saturated with argon, and the experiment was conducted under O_2-free atmosphere. Measurements were performed at room temperature (298 K). All the reagents and buffer electrolytes were of analytical grade (Sigma) and were prepared using Milli-Q water with a resistivity of 18 MΩ cm. CV experiments were performed in the +500 to 0 mV potential range at scan rates from 1 to 25 mV s^{-1}. Kinetics of *Bj*NirK with the physiological electron donor was assessed by chronoamperometry at an applied potential of 100 mV. The same methodology was used to perform kinetic tests of *Sm*NirK with its physiological electron donor pseudozurin (*Sm*Paz).[43] All the potential values are referred to SHE.

Spectroscopic methods

Absorption spectra were recorded at room temperature on a Shimadzu UV-1800 spectrophotometer.

X-band EPR measurements were performed on a Bruker EMX Plus spectrometer equipped with a universal high sensitivity cavity (HSW10819 model) using a Bruker nitrogen continuous-flow cryostat. Spectra were acquired under non-saturating conditions. Experimental: microwave frequency, 9.45 GHz; modulation field, 100 kHz; modulation amplitude, 2 Gpp; microwave power, 2 mW; temperature, 120K. EPR spectra were simulated with the EasySpin toolbox based on MATLAB® .[52]

Samples for EPR spectroscopy were concentrated to ~200 μM monomeric protein by using an Amicon device. Argon saturated solutions of sodium ascorbate and sodium dithionite were withdrawn with a gastight syringe from the vessels containing the respective solutions and loaded into argon-flushed EPR tubes containing protein samples (~ 200 μL) followed by gentle mixing. The EPR tubes were frozen with liquid nitrogen and stored under these conditions until use.

Computational methods

Since the X-ray structure of *Bj*NirK is not known, we performed a protein structure homology modelling using the SWISS-MODEL automated server.[53-56] The template structure used was *Br*^{2D}NirK (PDB 6THF) which shows 87 % of identity with *Bj*NirK.[14]

The hydrogen atoms and the protonation states at pH 7.0 of the titratable residues (*e.g.* His, Glu, Asp) were added using the empirical PROPKA procedure using the pdb2pqr server.[57] The structure was solvated with a shell of water molecules with 6 Å around the surface residues using the VMD program with default parameters.[58]

In order to neutralize the system, 9 Na^+ ions were added. A short molecular dynamics simulation was performed to relax the hydrogen atoms and the solvation water molecules by fixing the backbone atoms of all residues.

The combined quantum mechanics/molecular mechanics (QM/MM) calculations were performed as implemented in Gaussian 09 code.[59] For the QM part the spin-polarized WB97XD functional which includes empirical atom-atom dispersion corrections was used,[60] whereas the Amber classical force field for the MM part.[61] The basis set for the atoms in the QM part was 6-31G(d,p). We treated at the QM part the residues His328A, His121C, His156C, which are the ligands of the catalytic copper atom T2, His116C, His167C, Cys157C, which are nearest neighbors of copper atom at T1, and the weaker Met172C ligand, and the second sphere residues Asp119C (Asp_{CAT}), His277A (His_{CAT}), Gly171C, and Ser170C. To model the protein resting state a water molecule (H_2OA1) coordinated at T2-A, a water molecule (H_2OA2) close to Asp119C, and a water molecule (H_2OA3) bridging His_{CAT} and Asp_{CAT} were also included in the QM part. His_{CAT} was considered protonated at $N^{\delta 1}$ and $N^{\varepsilon 2}$, while Asp_{CAT} was deprotonated as suggested elsewhere.[31, 62] The structure was optimized with the QM residues free to relax and keeping fixed in position the atoms treated with MM. The rest of the residues were treated at the MM level of theory. The structure was optimized with the QM residues free to relax and keeping fixed in position the atoms treated at the MM part. The whole QM part structure including hydrogen atoms is giving as Electronic Supplementary Information (ESI). Additionally, time-dependent density functional theory (TDDFT) calculations using the HSEh1PBE functional and the basis set 6-31(d,p) were performed to rationalize both UV-vis spectra and type of covalency of T1.[63]

Results and discussion

Molecular and spectroscopic properties of *Bj*NirK

Molecular mass determination by gel filtration of *Bj*NirK yielded 116 kDa, whereas SDS-PAGE showed a band with molecular mass of ~ 40 kDa (see inset on Fig. 1). This indicates

a trimeric structure, as observed in *Sm*NirK [44] and NirKs from other sources.[1, 2] Metal analysis identified 2.0(1) Cu/monomer, indicating fully occupied T1 and T2 copper sites.

Fig. 1 shows the UV–vis absorption spectra of both *Bj*NirK and *Sm*NirK for comparison.[43] The spectrum of *Bj*NirK (blue solid line) shows two main absorption bands with maxima at 458 nm (ε = 2.6 mM^{-1} cm^{-1}) and 592 nm (ε = 4.4 mM^{-1} cm^{-1}). The $\varepsilon_{458}/\varepsilon_{592}$ ratio is 0.59, a bit lower than those reported for greenish-blue NirKs (0.8-1.0),[64-66] but higher than those of blue NirK (~ 0.2).[30, 67] *Sm*NirK (green solid line) and other green-type NirK show ratios higher than 1.1.[68, 69] Although the color of *Bj*NirK is blue, we tentatively classify *Bj*NirK within the greenish-blue NirK subgroup due to its $\varepsilon_{458}/\varepsilon_{592}$ ratio. The absorption spectrum of *Bj*NirK showed no significant differences in the 5-10 pH range (not shown), which indicates that T1 is not affected by any acid-base equilibrium in the cupric state, as reported for other NirK.[34, 43] The addition of either sodium ascorbate or sodium dithionite reduces the T1-Cu(II) to the cuprous state, leading to the disappearance of all visible absorption bands (not shown), as also previously described for green type *Sm*NirK.[44]

View Article Online
DOI: 10.1039/D0MT00177E

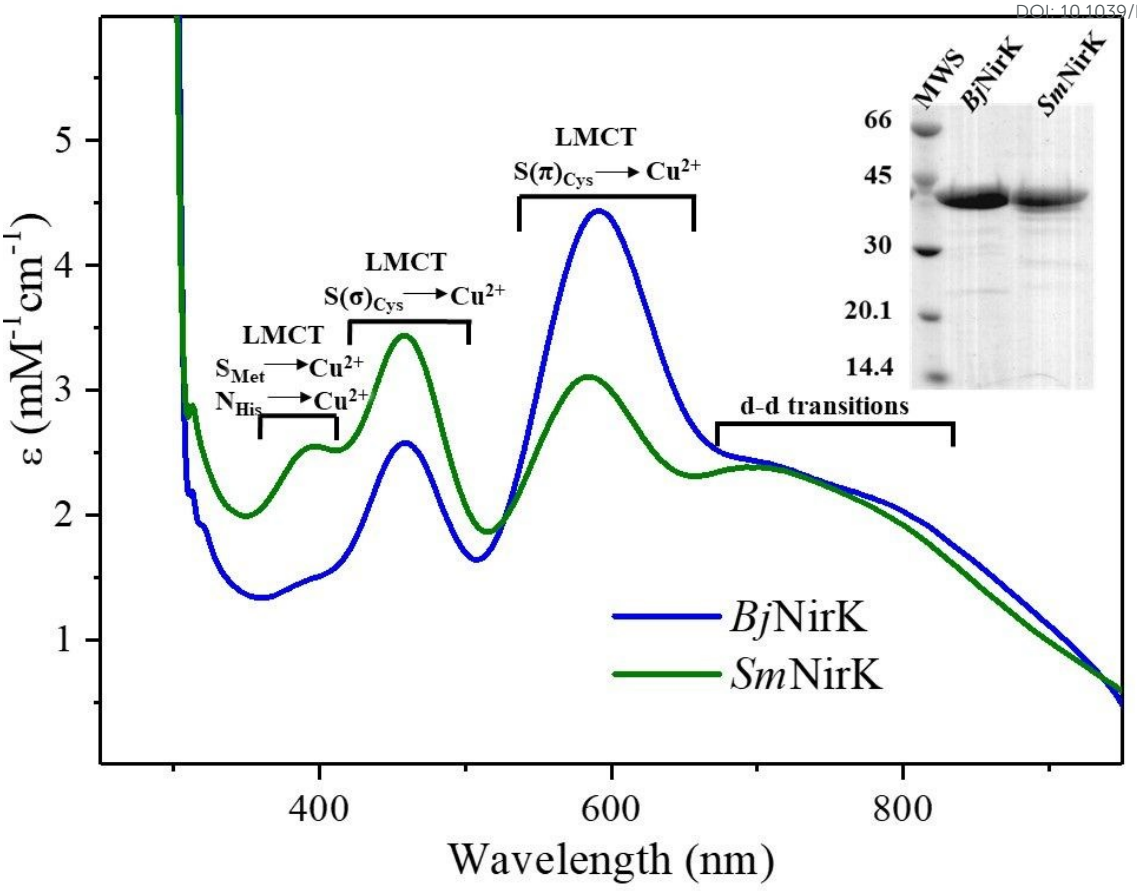

Fig.1 UV-vis absorption spectra of as-prepared *Bj*NirK and *Sm*NirK. The electronic transitions indicated on the figure are based on assignments reported elsewhere.[18] The inset shows the 12 % SDS-PAGE of both proteins.

Representative EPR spectra of *Bj*NirK obtained under different experimental conditions at pH 6.0 are shown in Fig. 2 (black solid lines). Spectrum "a" corresponds to as-prepared protein. Simulation of this spectrum (orange) was obtained assuming two overlapped nearly axial components associated with T1 (blue line, $g_{1,2,3} = 2.192, 2.052, 2.021$; $A_{//} = 7.1$ mT) and T2 (red line, $g_{1,2,3} = 2.315, 2.074, 2.064$, $A_{//} = 14.5$ mT). Spin quantification of as-prepared *Bj*NirK yielded ~ 2 spins/monomer, which indicates that both T1 and T2 are as Cu^{2+}. Upon sodium ascorbate addition, T1 is completely reduced to the diamagnetic Cu^{+} state, while ~

35 % of T2 remains as Cu^{2+} (spectrum "b"), indicating that $E°'$ of T2 is lower than that of T1. Addition of sodium dithionite excess relative to protein concentration under anaerobic conditions reduces completely both copper centers (spectrum "c") in line with reduction potentials falling in the range of 0 mV to + 300 mV *vs* SHE. The behavior towards ascorbate and dithionite of T1 and T2 is similar to that observed for *Sm*NirK, as well as in NirK from other sources.[20, 27, 34, 35, 64]

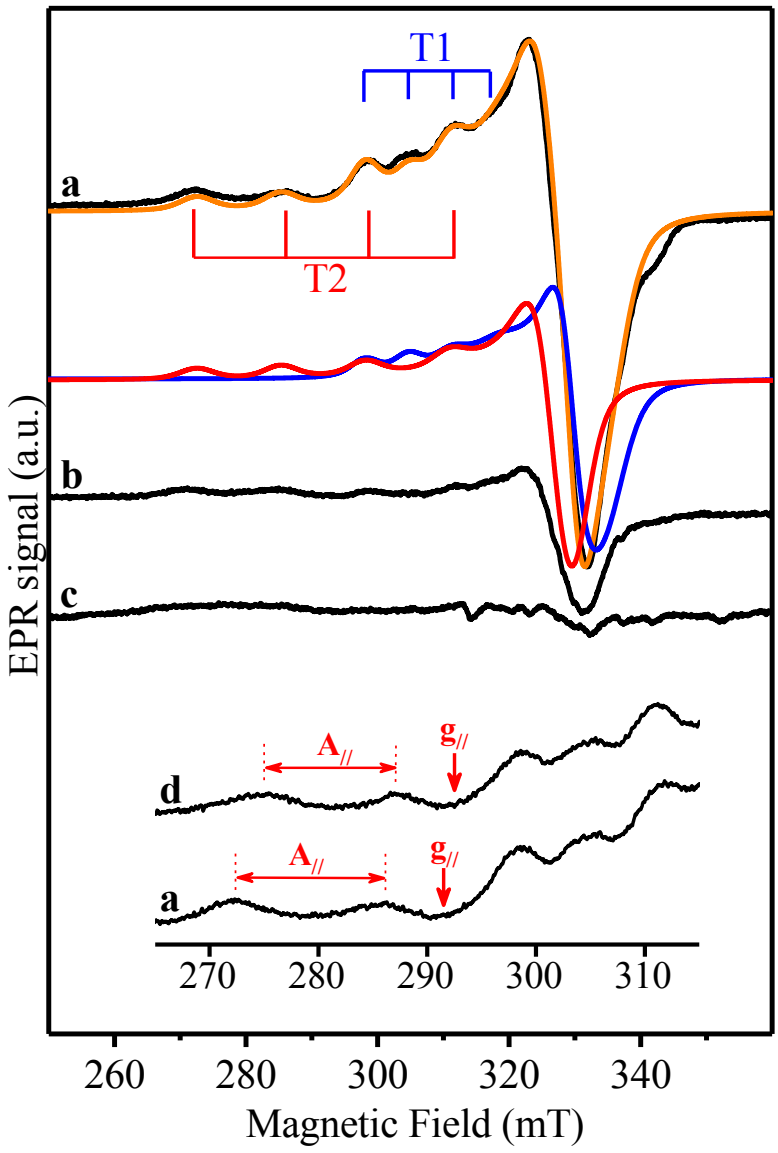

Fig. 2 EPR spectra of *Bj*NirK at pH 6.0. a) As-prepared *Bj*NirK (black solid line) together with simulation (orange solid line); simulation was obtained by adding T1 (blue) and T2 (red)

components in 1:1 ratio. b) As-prepared *Bj*NirK upon ascorbate addition in an ascorbate/protein ratio of ~ 5:1, c) As-prepared *Bj*NirK upon addition of excess dithionite in a dithionite/protein ratio of 20:1. The inset shows the changes in both $g_{//}$ and $A_{//}$ features of T2 upon addition of excess nitrite in a nitrite/protein ratio of 60:1 (spectrum "d") together with that of as-prepared enzyme (spectrum "a").

T1 EPR parameters of *Bj*NirK are highly similar to those of *Sm*NirK,[43] and indicates a Cu(II) d_{x2-y2} ground state in both enzymes. UV-vis data (Fig. 1) clearly show a different covalent interaction of the d_{x2-y2} copper orbital with the S(Cys) 3p orbitals, which is mostly of π-type in *Bj*NirK and of σ-type in *Sm*NirK. However, the almost identical T1 EPR features indicate that the S(Cys) 3p orbitals contribute with similar admixing factors to the ground state in both types of T1 sites. This observation is in line with Q-band ENDOR performed on *Rs*NirK, in which the green T1 of the wild type enzyme and the blue T1 of the same enzyme obtained by mutagenesis showed similar unpaired copper spin density onto the copper ligands.[70]

Since *Sm*NirK, as well as NirK from other sources, show slight modifications in both $g_{//}$ and $A_{//}$ values upon nitrite-T2 interaction,[35, 44, 64] we investigated the EPR behavior of *Bj*NirK at pH 6.0 upon sodium nitrite addition (see inset on Fig. 2). Whereas T1 EPR signal remains unchanged, that of T2 shows a behavior similar to that observed for *Sm*NirK, *i.e.* $g_{//}$ shifting to lower g-values ($g_{//}$= 2.307) and a decrease in the value of $A_{//}$ ($A_{//}$ = 13.3 mT) confirming that both proteins behave in a similar way towards substrate.

Reduction potential of the *Bj*NirK T1 determined by UV–vis mediated redox titration

Redox potentiometric titrations monitored by UV–vis were used to determine the reduction potential of T1 ($E°'$) by monitoring the intensity of typical electronic absorption bands as a function of potential (Fig. 3). Experimental data showed some deviations to the typical sigmoidal lineshape around the mid-point potential expected for a Nernstian behavior. Reasonable simulations of the data can be obtained assuming a pure Nernst model ($E°'$= 300 mV), but clearly shows that n, the number of electrons exchanged in the redox reaction, is greater than 1. This n-value > 1 for a one-electron reduction reaction, is in line with results obtained in *Achromobacter xylosoxidans* (*Ax*) NirK and *Geobacillus kaustophilus* HTA426 (*Gk*) NirK, for which n=1.5 and n= 1.9 have been reported, respectively.[4] Explanations such as ET from T1 to the optically "silent" T2 during titration in conjunction with the similar reduction potentials of both copper centers, and that T1→T2 ET operates through a gated mechanism, have been indicated as the causes for this n > 1 finding, but cannot explain the curve steepness we observe in our titration data. The analysis of this phenomenon is out of the scope of this paper, and will not be considered any further.

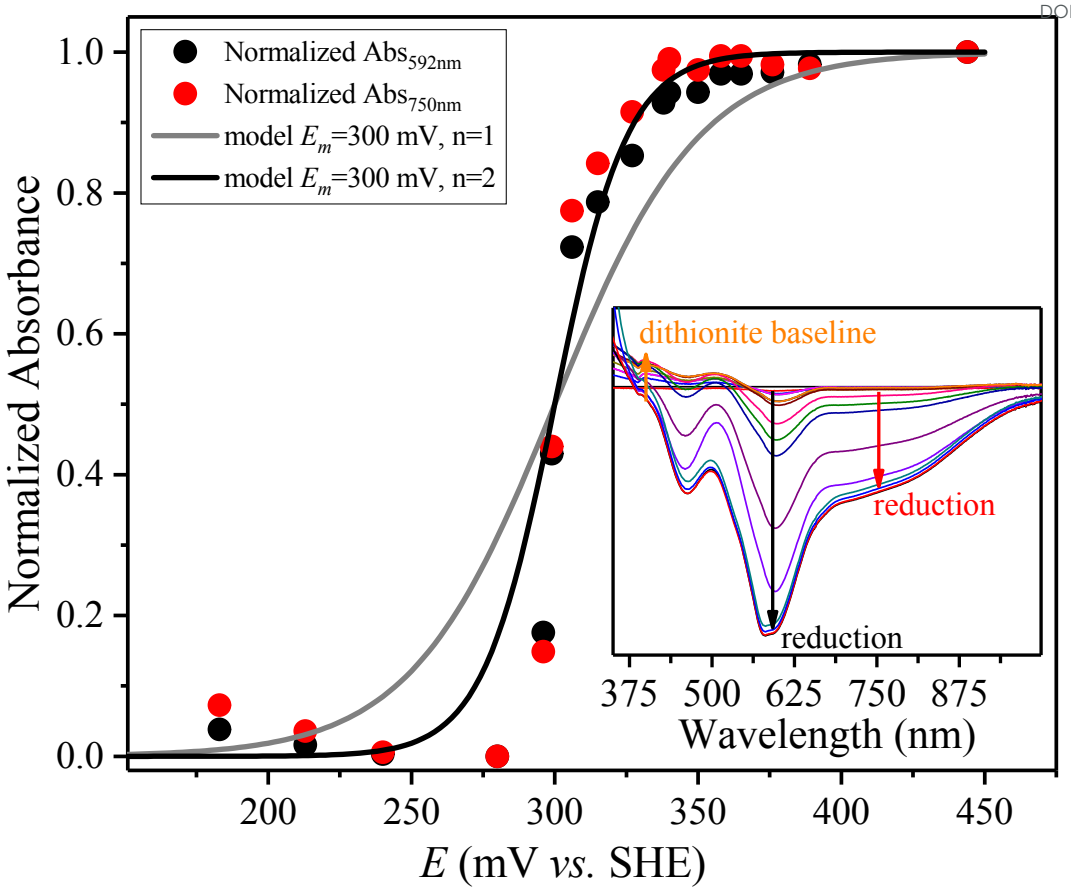

Fig. 3 Redox potentiometric titration of *Bj*NirK monitored by UV–vis spectroscopy. The changes of absorbance at both 592 and 750 nm (black and red circles, respectively) are plotted to show that baseline does not significantly affect the calculated $E°'$-value. The grey and black sigmoidal traces correspond to Nernst equation plots with n=1 and n=2, respectively. Inset: difference UV–vis spectra relative to the fully oxidized spectrum (E ~ 450 mV) at decreasing solution potentials. The black and red arrows indicate the change in absorbance at 592 and 750 nm, respectively. The orange arrow shows the baseline effect of dithionite absorbance, which only produces very small contributions at potentials lower than 250 mV.

View Article Online
DOI: 10.1039/D0MT00177E

Molecular, spectroscopic, and electrochemical properties of *Bj*CycA

Size-exclusion chromatography revealed the presence of three well defined peaks corresponding to molecular masses of ~ 14, 25, and 50 kDa (Fig. S1), whereas SDS-PAGE showed two close bands at ~ 14 kDa (see inset on Fig. 4). The comparison between both experiments suggests a concentration-dependent equilibrium in solution of monomers, dimers, and likely tetramers, as the level of aggregation depends on the concentration of the protein sample used in molecular-exclusion chromatography experiment (see Fig. S1 in ESI), the higher the concentration, the higher the aggregation. The presence of monomers is in line with reports that showed a monomer of 12.4 kDa.[71] The homodimeric arrangement is in line with cytochrome c_{550} from *Paracoccus denitrificans* which presents an equilibrium between monomers and dimers depending on the ionic strength of the protein solution,[72] and with studies on cytochrome *c*-549 and cytochrome c_6 from *Arthrospira maxima* that suggest that these proteins oligomerize.[73] The presence of two close bands in the SDS-PAGE gel (inset on Fig. 4) has also been observed for cytochromes from other sources and has been ascribed to partial degradation produced by DegP protease present in *E. coli* periplasm.[74] An alternative explanation could be that the lower molecular mass band corresponds to the mature protein while the bigger one might be unprocessed *Bj*CycA with signal peptide. Additional studies by complementary mass spectrometry techniques are necessary to confirm the oligomerization of *Bj*CycA in solution, and to elucidate the relevance of cytochrome aggregation in nitrite catalysis.

UV-vis spectrum of as-purified *Bj*CycA suggests that the heme iron is in the ferrous state (Fig. 4, red solid line) showing α, β and Soret bands at 550, 521 and 413 nm,

respectively. Addition of dithiothreitol under anaerobic conditions to as-purified *Bj*CycA modifies slightly the spectrum increasing the intensity of α, β and Soret bands without significant shifting (not shown), confirming that as-purified *Bj*CycA is mostly obtained in the reduced form. The UV-vis spectrum of the oxidized Fe^{3+} form of *Bj*CycA (black solid line) shows a Soret peak at 410 nm, and was obtained upon redox cycling the protein in the presence of both nitrite and *Bj*NirK (*Bj*CycA/*Bj*NirK ratio of 100:1).

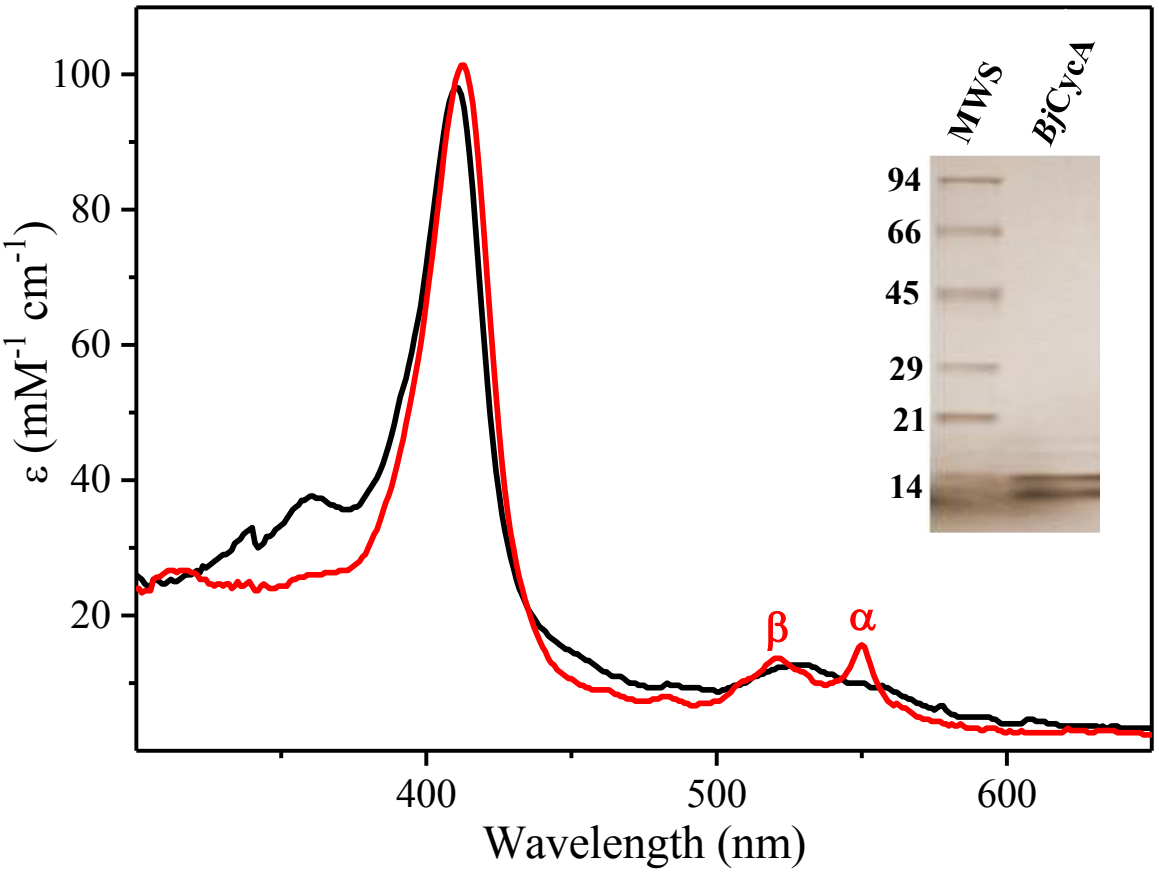

Fig. 4 UV-vis absorption spectra of reduced (*as-purified*, red solid line) and oxidized (black solid line) forms of *Bj*CycA. The inset shows the 15 % SDS-PAGE of *Bj*CycA.

Cyclic voltammograms showed a reversible response characterized by cathodic and anodic peaks with same intensity, showing ΔE_{peak} ~ 35 mV (see Fig. S2 in ESI). The half-

height peak width was about 90 mV for both cathodic and anodic peaks at scan rates lower than 10 mV/s, indicating a reversible one-electron process.[75] The formal reduction potential [$E^{\circ\prime} = (E_{pc} + E_{pa})/2$] was determined to be $E^{\circ\prime} = 265$ (7) mV *vs* SHE, which is in line with potential values determined elsewhere,[71] and for *c*-type cytochromes from other sources.[76]

Kinetic studies

Steady-state kinetics of *Bj*NirK using MV as non-physiological electron donor yielded k_{cat}=10.6 (4) s^{-1} and K_m = 900 (200) μM. The catalytic activity is lower than that reported for the green-type *Sm*NirK using the same methodology (k_{cat}= 240 (50) s^{-1} and K_m= 3600 (300) μM).[43] *Bj*NirK activity is of the same order of magnitude reported for the NirK from *Bradyrhizobium* sp. ORS 375 (*Br*^{2D}NirK),[14] which shows 87% of amino acid sequence identity with *Bj*NirK. The catalytic activities of *Bj*NirK and *Br*^{2D}NirK represent respectively ~ 1% and 5 % of activities reported for the blue class I *Ax*NirK.[4]

The kinetic ability of *Bj*NirK using the physiological electron donor *Bj*CycA was tested by chronoamperometry using the same methodology reported for the couple *Sm*NirK/*Sm*Paz.[43] Although *Bj*NirK does not yield faradaic currents on a gold electrode in absence or in presence of nitrite, *Bj*CycA does (Fig. S2). Therefore, when both proteins are confined with a dialysis membrane close to the surface of the working electrode, *Bj*NirK is able to catalyze nitrite reduction receiving electrons from *Bj*CycA, which mediates ET from the gold electrode. Fig. 5 shows a chronoamperogram obtained with this setup, where increasing amounts of $NaNO_2$ were sequentially added; the results obtained for *Sm*NirK are included for comparison.[43] A Hanes-Woolf plot assuming a Michaelis-Menten model (see inset on Fig. 5) yielded an apparent K_m of 210(10) μM and i_{max}= 0.81(1) μA. The apparent k_{cat} value could not be calculated because the *Bj*CycA+*Bj*NirK instability hampered us to

determine the concentration of redox active protein at the electrode,[77] which precludes the comparison with the *Sm*NirK/*Sm*Paz couple results. However, the current intensities upon successive nitrite additions (Fig. 5) were smaller in *Bj*NirK/*Bj*CycA than those observed for *Sm*NirK/*Sm*Paz using the same setup, which is in line with the kinetic studies in solution.

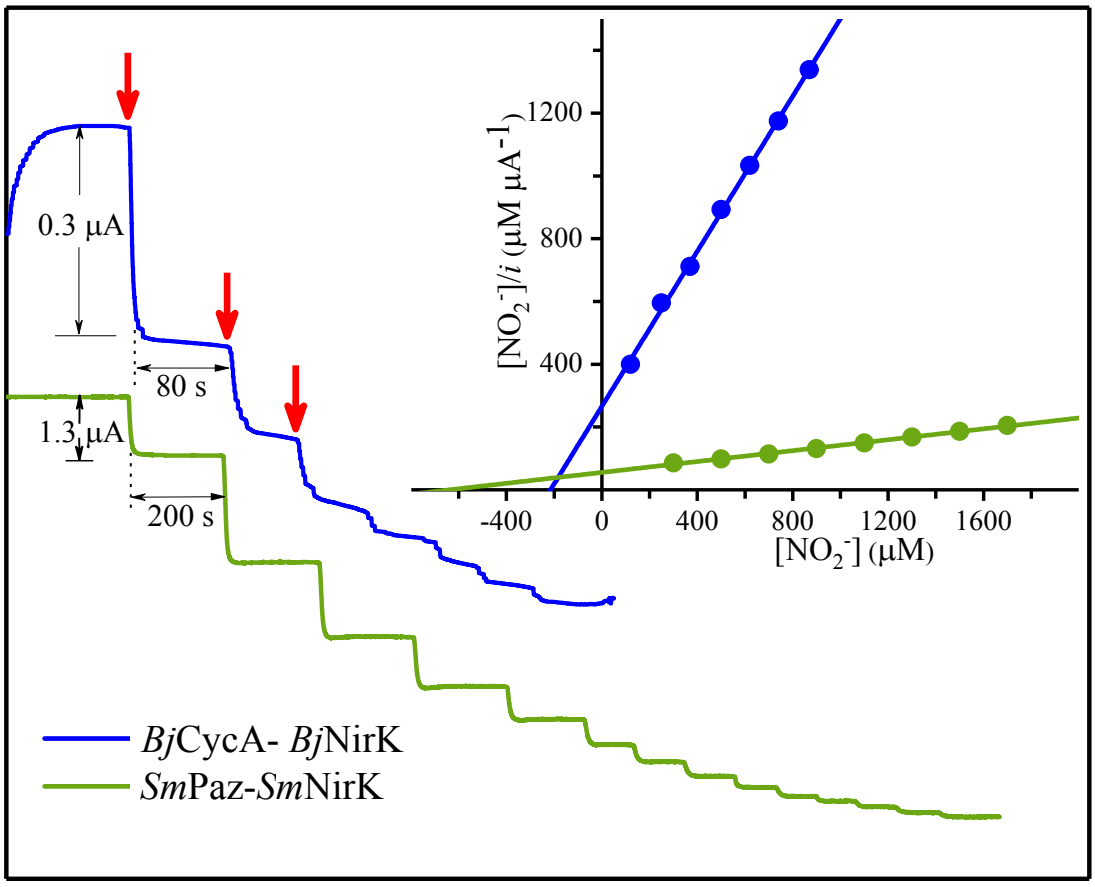

Fig. 5 Chronoamperogram of *Bj*NirK/*Bj*CycA together with that of *Sm*NirK/*Sm*Paz for comparison. Data analysis through Hanes-Woolf plot (see inset) yielded K_m^{app} = 210(10) µM and i_{max}= 0.81(1) µA for *Bj*NirK/*Bj*CycA and K_m^{app} = 610(20) µM and i_{max}= 11.5(1) µA for *Sm*NirK/*Sm*Paz.[43] Red arrows indicate some points of nitrite addition. Chronoamperograms were corrected for protein denaturation and electrode surface passivation according to Fourmond et al.[78]

Structural features linked to low catalytic efficiency

QM/MM calculations were performed based on a homology model constructed from a reported crystallographic structure of *Br*^{2D}NirK (PDB 6THF),[14] as described under Computational Methods. *Bj*NirK and *Br*^{2D}NirK share 87 % amino acid sequence identity including signal peptide. The resulting *Bj*NirK QM/MM model with Cu^{2+} ions is presented in panel A of Fig. 6 superimposed to the X-ray crystal structures of the greenish-blue *Br*^{2D}NirK ($\varepsilon_{462}/\ \varepsilon_{591}$ = 0.58), and the blue type *Ax*NirK (PDB 1OE1).[79] The structure of *Ax*NirK is included because these two greenish-blue enzymes present absorption properties close to blue NirK. As shown in Fig. 6, the three structures are highly similar for the atoms considered in the QM part and all the water molecules included in our model (See Fig. S3 in ESI for details of the QM calculation). Furthermore, it is important to note that the T1 structures of *Bj*NirK and *Br*^{2D}NirK do not show significant differences with that of *Ax*NirK, in line with the T1 UV-vis spectra of *Bj*NirK (Fig. 1) and *Br*^{2D}NirK.[14]

View Article Online
DOI: 10.1039/D0MT00177E

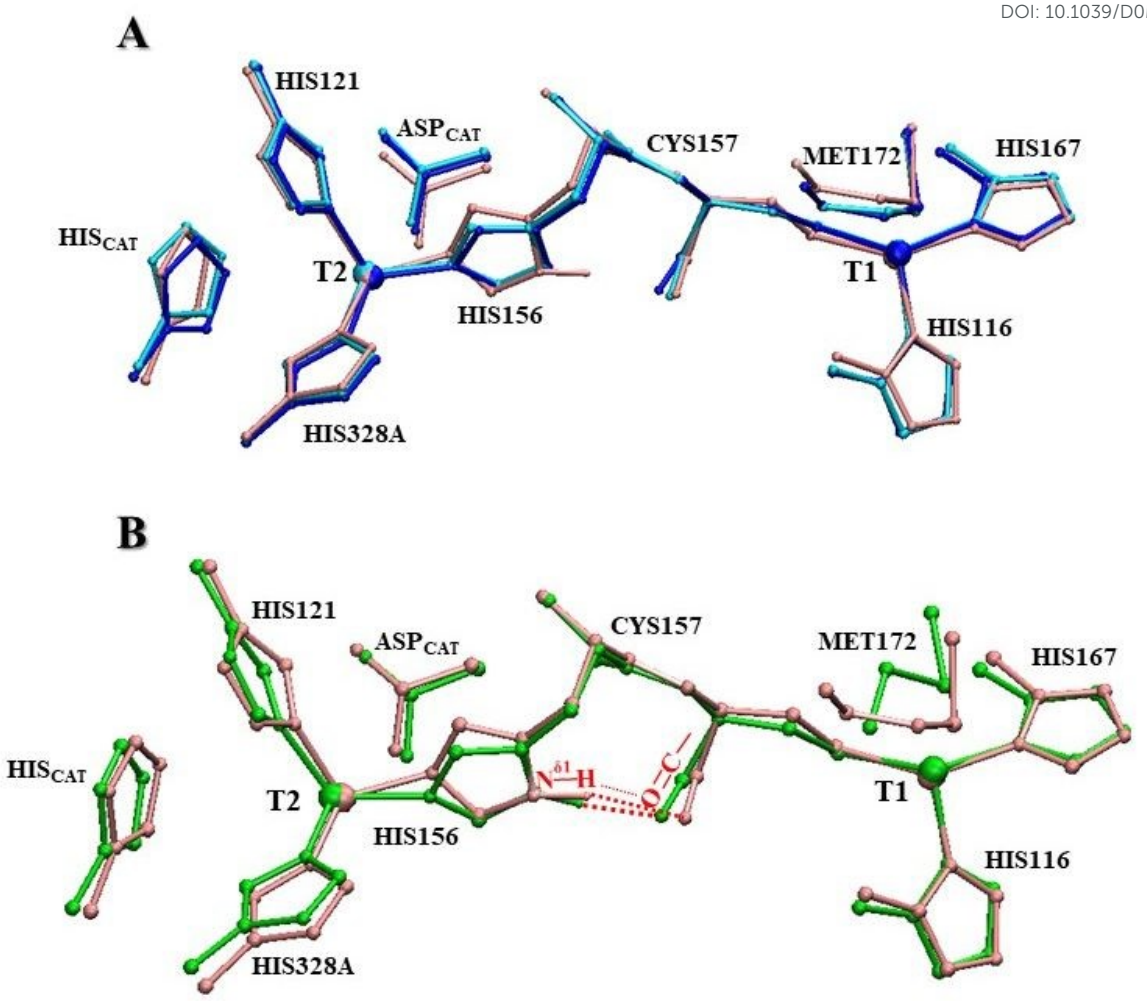

Fig. 6 A) Superposition of optimized QM/MM structure of *Bj*NirK (pink) with the X-ray structure of *Br*^{2D}NirK (light blue, PDB 6THF) and *Ax*NirK (blue, PDB 1OE1). B) Superposition of optimized QM/MM structures of *Bj*NirK (pink) with that of *Sm*NirK (green).[43] Only atoms treated by QM are shown. Labels are in *Bj*NirK numbering. Hydrogen atoms were omitted for clarity.

Panel B of Fig. 6 shows a superposition of the optimized QM/MM structures of *Bj*NirK (pink) and *Sm*NirK (green). T1 first coordination spheres of *Bj*NirK and *Sm*NirK show the typical characteristics that differentiate blue and green T1; the Cu-S(Met) bond of blue T1 is

longer than that of green T1 (2.70 Å *vs* 2.57 Å) and different angles between S(Met)-Cu-S(Cys) and N(His)-Cu-N(His) planes angles (104 ° *vs* 62 °). Unexpectedly, both T1 presented similar Cu-S(Cys) bond distances (2.18 Å and 2.16 Å). The rest of the amino acid residues as well as their non-covalent interactions proposed to be relevant to catalysis, are highly conserved in each model, *e.g.* the T2Cu-H2O-Asp_{CAT}-H2O(bridging)-His_{CAT} and the H-bond between $N^{\delta 1}$ of T2 His ligand and the carbonyl O atom of Cys coordinated to T1 of the Cys-His bridge (Fig. S3 in ESI).

The similar Cu-S(Cys) bond lengths of *Bj*NirK and *Sm*NirK is in line with the available structural data of NirK reported so far,[15] but in contradiction with the coupled distortion model proposed to rationalize the absorption spectra of T1 centers.[80] Hence, we performed TDDFT calculations using a smaller model of the T1 sites of both enzymes to give additional support to the structures shown in panel B of Fig. 6. As shown in Fig. S4 (ESI), these calculations reproduced reasonably well the S(Cys)→Cu LMCT transitions of the visible absorption spectra shown in Fig. 1, confirming the validity of both QM/MM models.

Despite the redox and structural properties of T1 and T2 and the behavior towards nitrite of T2 of *Bj*NirK are similar to those reported in other NirK, the enzyme presents enzymatic activity about two orders of magnitude lower than that of *Ax*NirK (see kinetic studies section), similar to that observed for the homologue *Br*^{2D}NirK.[14] This observation cannot be ascribed to an inefficient ET between *Bj*CycA and T1-*Bj*NirK, as the reduction potential gradient from *Bj*CycA heme ($E°'$=265 mV) to *Bj*NirK T1 ($E°'$=303 mV) is favorable, as also observed for the *Ax*Cytc_{551}/*Ax*NirK pair ($E°'$ of 241 mV and 280 mV, respectively).[76] The comparison of the primary sequences of *Bj*NirK and *Br*^{2D}NirK with other class I NirK shows that the loop Cys130-Met145 (Cys157-Met172 in *Bj*NirK) adjacent to T1, a protein loop involved in the interaction with the physiological electron donor,[24] contains one extra proline

residue. On the basis of kinetic, mutagenesis, and structural studies of *Ax*NirK, the extra residue was suggested to cause higher loop flexibility, and hence low enzyme activity.[14, 20, 81] In both *Bj*NirK and *Br*^{2D}NirK, this extra proline residue should also produce a similar effect, which would eventually lead to a higher flexibility. Molecular dynamic studies are necessary to give an extra support to this hypothesis.

Effect of pH on T1-T2 electron transfer

Fig. 7 shows UV-vis and EPR spectra at pH 6.0 and 10.0. UV-vis and EPR spectra of T1 at pH 6.0 and 10.0 do not show significant modifications, unless of some broadening of EPR resonance lines at high pH, which suggests a certain degree of protein disorder at T1. T2 shows a single EPR spectral component at pH 6.0 (Fig. 2 and Fig. 7) but two overlapping EPR signals at pH 10.0. The two EPR signals at high pH, which are distinct to that at pH 6, are in a ratio of 4:1 and are identified as I (major component; $g_{//} = 2.231$, $A_{//} = 20.6$ mT) and II (minor component; $g_{//} = 2.345$, $A_{//} = 16$ mT) (See Fig. S5 in ESI for simulation details). Similar results were obtained using ascorbate as reductant (Fig. S6). This indicates a remarkably T2 pH-dependent structural anisotropy, which is more important than that of T1. These pH-dependent structural changes are reversible, as both T1 and T2 EPR signals as well as catalytic activity are recovered when the pH is lowered from 10.0 to 6.0, confirming that the enzyme structure is not irreversible affected by the alkaline conditions. Although with a distinct ratio, two T2 EPR components were also observed in *Sm*NirK (major component, $g_{//} = 2.345$ and $A_{//} = 11.5$ mT; minor component, $g_{//} = 2.231$ and $A_{//} = 20.7$ mT),[43] indicating that both *Bj*NirK and *Sm*NirK behave similarly. Changes in the T2 EPR signal at high pH were also detected in *Rs*NirK, for which a second spectral component ($g_{//,\perp} = 2.35, 2.09$; $A_{//} = 9.5$ mT) coexisting with the low pH one ($g_{//,\perp} = 2.31, 2.07$; $A_{//} = 15$ mT) was detected at pH 8.4;[34]

the reduction potential of the copper species associated with the second spectral component (137 mV) was determined to be 81 mV lower than that of the low pH species (218 mV). The *Sm*NirK and *Bj*NirK structural anisotropy at T2 suggested by EPR is in line with EPR and the crystal structure of *Rs*NirK at pH 8.4.[34] This structure was solved assuming two different protein conformations, which was suggested to constitute a simplification of the full motion experienced by the protein at high pH. In summary, all the above experiments indicate a pH-dependent increase in the disorder of the protein structure at level of the essential residues for catalysis, which is reverted upon lowering pH to the value of enzyme maximal activity.

View Article Online
DOI: 10.1039/D0MT00177E

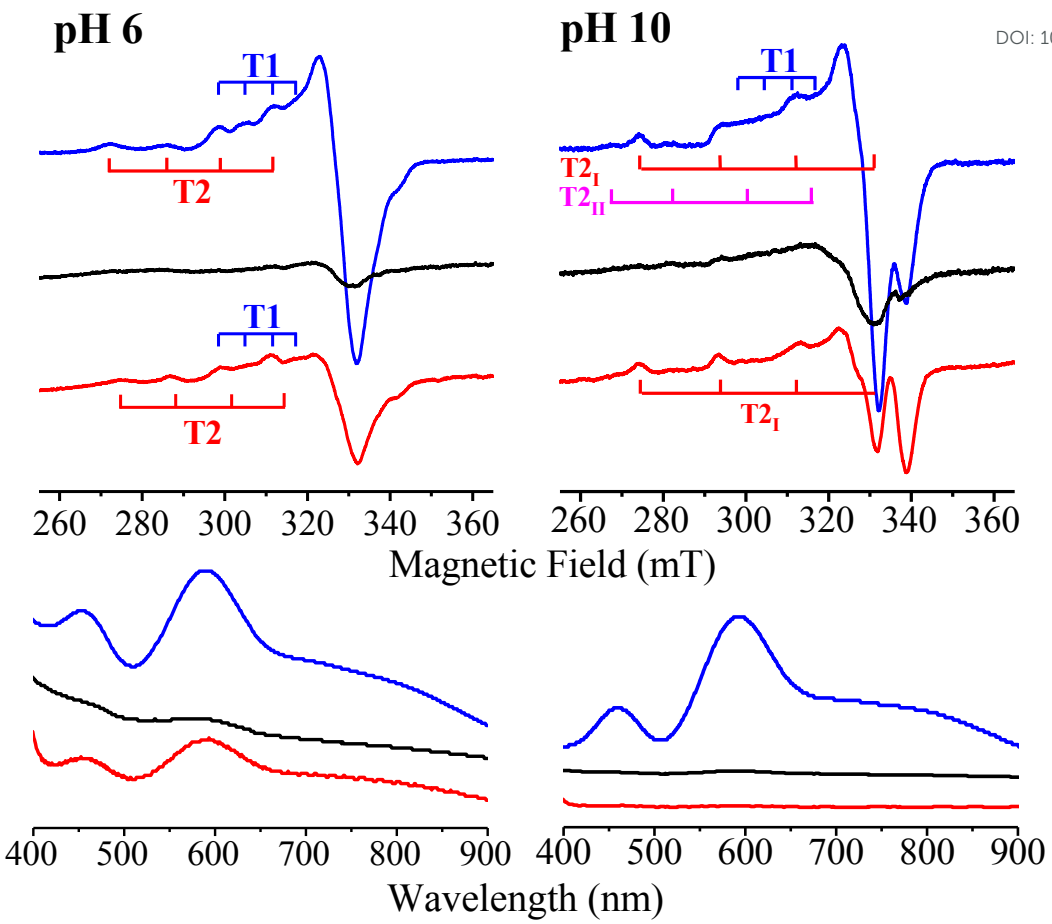

Fig. 7 Reoxidation experiments of dithionite-reduced *Bj*NirK at pH 6.0 and 10.0 (left and right panels, respectively) monitored by EPR (upper) and UV-vis (lower) spectroscopies upon sodium nitrite addition. Blue spectra, as-purified *Bj*NirK; black spectra, dithionite reduced *Bj*NirK; Red spectra, dithionite reduced *Bj*NirK upon addition of nitrite excess (nitrite:dithionite ratio of 5:1). Subindexes I and II identify the two T2 components observed at high pH, see more details in Fig. S5 in ESI.

We then evaluated the kinetic ability of the dithionite-reduced enzyme at pH 6.0 and 10.0 by monitoring the oxidation state of each copper center after redox cycling the enzyme with nitrite using dithionite as electron donor. The reaction was conducted in the presence of nitrite excess relative to dithionite (ratio of 5:1) and the oxidation state of each copper center was

monitored after 10 min of incubation, a time long enough to assure that dithionite was fully consumed at pH 6.0. Under these conditions, the detection of a reoxidized copper T2 center is indicative of nitrite reduction, whereas the simultaneous detection of reoxidized T1 and T2 centers would indicate not only nitrite reduction, but also T1-T2 ET. Left panels of Fig. 7 show these experiments at pH 6.0. The fact that T1 and T2 can be observed in the Cu^{2+} state upon nitrite addition (red spectra) confirms nitrite/T2 interaction, T2 oxidation after nitrite reduction, and T1-T2 ET. In contrast, the same experiment conducted at pH 10.0 (right panels) shows the EPR signal of Cu^{2+}-T2, but not that of Cu^{2+}-T1 (red spectra). The same outcome is obtained if nitrite is added before dithionite. The EPR-monitored experiment at pH 10.0 clearly indicates that the T2 center reacts with nitrite to yield Cu^{2+}-T2, whereas the absence of spectroscopic features associated with oxidized T1 confirms the absence of T1-T2 ET. Furthermore, these results would confirm that proton delivery for nitrite reduction is kept at high pH, otherwise the enzyme could not be reoxidized, and hence the original T2 EPR signal should not be observed. Similar results were obtained for the green type *Sm*NirK.[43] This indicates that nitrite reduction at high pH is produced in a T1-decoupled way if reducing equivalents are directly supplied to T2. The latter observation but at pH 6.0 was also shown to occur in C172D, a variant of *Sm*NirK that lacks a functional T1 center which catalyze nitrite at very low rates.[43]

Nitrite reoxidation experiments performed on both *Sm*NirK and *Bj*NirK show some resemblance with pH drop experiments performed on nitrite-bound *Rs*NirK using ascorbate as reductant.[36] pH drop experiments showed that T1 is reduced at high pH using ascorbate but not nitrite-bound T2, which was ascribed to the lack of T1→T2 ET provoked by a decrease in the T2 reduction potential of nitrite-bound T2 (at least 120 mV lower than that of T1, $E°' = 247$ mV). Furthermore, it was additionally postulated that high pH precludes

proton delivery to reduce nitrite. A similar suggestion was proposed from a redox titration of *Rs*Nirk at pH 8.4 using ascorbate as reductant that showed that T2 presents a reduction potential only 81 mV lower than that of T1.[34] We checked by EPR and UV-vis the behavior towards ascorbate of *Sm*NirK and *Bj*NirK at pH 10. For both enzyme without nitrite, ascorbate reduces completely T1 copper centers and approximately ~ 70 % of T2 centers (Fig. S6), which suggests that reduction potentials at high pH are not significantly modified relative to those at pH 6. Thus, the experiments using ascorbate and dithionite as electron donors suggest that in both *Sm*NirK and *Bj*NirK the lack of T1-T2 ET at high pH is not associated with an unfavorable driving force, but other factors should be taken into account.

The fact that both *Sm*NirK and *Bj*NirK at high pH reduce nitrite in a T1 decoupled way indicates that T1-T2 ET is suppressed at high pH irrespective of the type of the Cu-S(Cys) covalent bond at T1. As seen above, the Cys-His bridge is formed by a pure covalent pathway additionally stabilized by a H-bond bridge that shortcuts the T1-T2 covalent link. Crystal structures of *Rs*NirK with and without nitrite at high and low pH do not show significant changes in the Cys-His bridge pure covalent pathway, but a shortening at high pH in the donor-acceptor distance of the $N^{\delta 1}H\ldots O{=}C$ hydrogen bond ($\Delta d_{D\text{-}A}$ of 0.3 and 0.2 Å for the resting and nitrite-bound *Rs*NirK, respectively).[34] As seen above, our EPR studies in both *Bj*NirK and *Sm*NirK show an increased T1 and T2 disorder at high pH, which should impact on the Cys-His bridge conformation. Then, it is conceivable that a likely cause that precludes ET at high pH is the increased protein disorder with pH in our enzymes. Our current hypothesis is that the $N^{\delta 1}H\ldots O{=}C$ hydrogen bond is more susceptible to be perturbed than the rigid covalent pathway, which is in line with the available structural data on *Rs*NirK.[34] Additional work is necessary to confirm this hypothesis.

Conclusions

A two domain copper-containing NirK and its physiological electron donor from *B. japonicum* were cloned, overexpressed, purified, and characterized to study whether the type of covalency of T1 influences the intraprotein long-distance electron transfer necessary for nitrite reduction and how the Cys-His bridge is involved in the pH-dependent catalytic activity of NirK. The results obtained for this enzyme were compared with those of *S. meliloti* NirK, which we had previously characterized. UV-vis and EPR studies complemented with computational calculations showed d_{x2-y2} ground states with different covalencies in the T1 centers of both enzymes. This is reflected in the absorption properties of T1, which are mainly determined by S(Cys)3pπ→Cu^{2+} and S(Cys)3pσ→Cu^{2+} LMCT transitions in *Bj*NirK and *Sm*NirK, respectively. TDDFT calculations confirm that the different type of covalency of the T1 sites of both enzymes is not associated with changes in the length of Cu-S(Cys) bond.

The physiological electron donor of *Bj*NirK, *Bj*CycA, was also characterized. *Bj*CycA is a cytochrome c_{550} in which the heme iron is obtained in the ferrous state in the as-purified form owing to its high reduction potential. *Bj*NirK shows low enzymatic activity compared to *Sm*NirK and classical class I NirK in general, which is likely due to the higher flexibility of a protein loop associated with *Bj*NirK/*Bj*CycA interaction. *Bj*NirK, like green *Sm*NirK, catalyzes nitrite reduction at high pH using the non-physiological electron donor dithionite. The kinetic reaction at high pH is conducted in a T1-decoupled way where nitrite reduction is entirely performed at T2 and proton delivery for nitrite reduction is maintained. We observed that the lack of T1-T2 ET at high pH does not depend of the type of Cu-S(Cys) covalency of T1. The increased disorder experienced by both copper centers which should impact on the Cys-His bridge seems to be the likely cause that precludes ET at high pH.

View Article Online
DOI: 10.1039/D0MT00177E

Conflicts of interests

There are no conflicts to declare.

Acknowledgments

We thank FONCyT, CONICET, and CAI+D-UNL for financial support. M.G.R., P.J.G, S.D.D., F.M.F. and C.D.B are members of CONICET (Argentina). J.C.C. and A.B.D. thank CONICET for fellowship grants.

References

1. W. G. Zumft, Cell biology and molecular basis of denitrification, *Microbiol. Mol. Biol. Rev.*, 1997, **61**, 533-616.
2. B. A. Averill, Dissimilatory Nitrite and Nitric Oxide Reductases, *Chem. Rev.*, 1996, **96**, 2951-2964.
3. M. Kukimoto, M. Nishiyama, M. E. P. Murphy, S. Turley, E. T. Adman, S. Horinouchi and T. Beppu, X-ray Structure and Site-Directed Mutagenesis of a Nitrite Reductase from Alcaligenes Faecalis S-6: Roles of Two Copper Atoms in Nitrite Reduction, *Biochemistry*, 1994, **33**, 5246-5252.
4. Y. Fukuda, H. Koteishi, R. Yoneda, T. Tamada, H. Takami, T. Inoue and M. Nojiri, Structural and functional characterization of the Geobacillus copper nitrite reductase: involvement of the unique N-terminal region in the interprotein electron transfer with its redox partner, *Biochim. Biophys. Acta*, 2014, **1837**, 396-405.
5. E. Libby and B. A. Averill, Evidence that the Type 2 copper centers are the site of nitrite reduction by Achromobacter cycloclastes nitrite reductase, *Biochem. Biophys. Res. Commun.*, 1992, **187**, 1529-1535.
6. S. Suzuki, T. Kohzuma, Deligeer, K. Yamaguchi, N. Nakamura, S. Shidara, K. Kobayashi and S. Tagawa, Pulse Radiolysis Studies on Nitrite Reductase from Achromobacter cycloclastes IAM 1013: Evidence for Intramolecular Electron Transfer from Type 1 Cu to Type 2 Cu, *J. Am. Chem. Soc.*, 1994, **116**, 11145-11146.
7. T. Inoue, M. Gotowda, Deligeer, K. Kataoka, K. Yamaguchi, S. Suzuki, H. Watanabe, M. Gohow and Y. Kai, Type 1 Cu structure of blue nitrite reductase from Alcaligenes xylosoxidans GIFU 1051 at 2.05 Å resolution: Comparison of blue and green nitrite reductases, *J. Biochem.*, 1998, **124**, 876-879.
8. F. E. Dodd, J. Van Beeumen, R. R. Eady and S. S. Hasnain, X-ray structure of a blue-copper nitrite reductase in two crystal forms. The nature of the copper sites, mode of substrate binding and recognition by redox partner, *J. Mol. Biol.*, 1998, **282**, 369-382.
9. S. Suzuki, K. Kataoka and K. Yamaguchi, Metal coordination and mechanism of multicopper nitrite reductase, *Acc. Chem. Res.*, 2000, **33**, 728-735.
10. M. Nojiri, Y. Xie, T. Inoue, T. Yamamoto, H. Matsumura, K. Kataoka, Deligeer, K. Yamaguchi, Y. Kai and S. Suzuki, Structure and function of a hexameric copper-containing nitrite reductase, *Proc. Natl. Acad. Sci. U.S.A.*, 2007, **104**, 4315-4320.
11. S. V. Antonyuk, H. Cong, R. R. Eady and S. S. Hasnain, Structures of protein-protein complexes involved in electron transfer, *Nature*, 2013, **496**, 123-126.
12. A. Tsuda, R. Ishikawa, H. Koteishi, K. Tange, Y. Fukuda, K. Kobayashi, T. Inoue and M. Nojiri, Structural and mechanistic insights into the electron flow through protein for cytochrome c-tethering copper nitrite reductase, *J. Biochem.*, 2013, **154**, 51-60.
13. D. J. Opperman, D. H. Murgida, S. D. Dalosto, C. D. Brondino and F. M. Ferroni, A three-domain copper-nitrite reductase with a unique sensing loop, *IUCrJ*, 2019, **6**, 248-258.
14. D. Sasaki, T. F. Watanabe, R. R. Eady, R. C. Garratt, S. V. Antonyuk and S. S. Hasnain, Reverse protein engineering of a novel 4-domain copper nitrite reductase reveals functional regulation by protein-protein interaction, *FEBS J.*, 2020, **n/a**.

15. M. Nojiri, in *Metalloenzymes in denitrification: applications and environmental impacts*, eds. I. Moura, J. J. Moura, S. R. Pauleta and L. B. Maia, Royal Society of Chemistry, Cambridge CB4 0WF, UK, 2016, vol. 9, ch. 5, pp. 91-113.
16. S. Suzuki, K. Kataoka, K. Yamaguchi, T. Inoue and Y. Kai, Structure–function relationships of copper-containing nitrite reductases, *Coord. Chem. Rev.* , 1999, **190–192**, 245-265.
17. S. Ghosh, X. Xie, A. Dey, Y. Sun, C. P. Scholes and E. I. Solomon, Thermodynamic equilibrium between blue and green copper sites and the role of the protein in controlling function, *Proc. Natl. Acad. Sci. U.S.A.*, 2009, **106**, 4969-4974.
18. E. I. Solomon and R. G. Hadt, Recent advances in understanding blue copper proteins, *Coord. Chem. Rev.* , 2011, **255**, 774-789.
19. A. C. Merkle and N. Lehnert, Binding and activation of nitrite and nitric oxide by copper nitrite reductase and corresponding model complexes, *Dalton Trans.*, 2012, **41**, 3355-3368.
20. N. G. H. Leferink, C. Han, S. V. Antonyuk, D. J. Heyes, S. E. J. Rigby, M. A. Hough, R. R. Eady, N. S. Scrutton and S. S. Hasnain, Proton-coupled electron transfer in the catalytic cycle of Alcaligenes xylosoxidans copper-dependent nitrite reductase, *Biochemistry*, 2011, **50**, 4121-4131.
21. S. Horrell, D. Kekilli, R. W. Strange and M. A. Hough, Recent structural insights into the function of copper nitrite reductases, *Metallomics*, 2017, **9**, 1470-1482.
22. W. G. Zumft, D. J. Gotzmann and P. M. Kroneck, Type 1, blue copper proteins constitute a respiratory nitrite-reducing system in Pseudomonas aureofaciens, *Eur. J. Biochem.*, 1987, **168**, 301-307.
23. F. E. Dodd, S. S. Hasnain, W. N. Hunter, Z. H. Abraham, M. Debenham, H. Kanzler, M. Eldridge, R. R. Eady, R. P. Ambler and B. E. Smith, Evidence for two distinct azurins in Alcaligenes xylosoxidans (NCIMB 11015): potential electron donors to nitrite reductase, *Biochemistry*, 1995, **34**, 10180-10186.
24. M. Nojiri, H. Koteishi, T. Nakagami, K. Kobayashi, T. Inoue, K. Yamaguchi and S. Suzuki, Structural basis of inter-protein electron transfer for nitrite reduction in denitrification, *Nature*, 2009, **462**, 117-120.
25. T. Kakutani, H. Watanabe, K. Arima and T. Beppu, A blue protein as an inactivating factor for nitrite reductase from Alcaligenes faecalis strain S-6, *J. Biochem.*, 1981, **89**, 463-472.
26. M. Y. Liu, M. C. Liu, W. J. Payne and J. Legall, Properties and electron transfer specificity of copper proteins from the denitrifier "Achromobacter cycloclastes", *Journal of bacteriology*, 1986, **166**, 604-608.
27. F. M. Ferroni, J. Marangon, N. I. Neuman, J. C. Cristaldi, S. M. Brambilla, S. A. Guerrero, M. G. Rivas, A. C. Rizzi and C. D. Brondino, Pseudoazurin from Sinorhizobium meliloti as an electron donor to copper-containing nitrite reductase: influence of the redox partner on the reduction potentials of the enzyme copper centers, *J. Biol. Inorg. Chem.*, 2014, **19**, 913-921.
28. R. G. Hadt, S. I. Gorelsky and E. I. Solomon, Anisotropic Covalency Contributions to Superexchange Pathways in Type One Copper Active Sites, *J. Am. Chem. Soc.*, 2014, **136**, 15034-15045.
29. M. J. Boulanger, M. Kukimoto, M. Nishiyama, S. Horinouchi and M. E. P. Murphy, Catalytic Roles for Two Water Bridged Residues (Asp-98 and His-255) in the

Active Site of Copper-containing Nitrite Reductase, *J. Biol. Chem.*, 2000, **275**, 23957-23964.

30. K. Kataoka, H. Furusawa, K. Takagi, K. Yamaguchi and S. Suzuki, Functional Analysis of Conserved Aspartate and Histidine Residues Located Around the Type 2 Copper Site of Copper-Containing Nitri Reductase1, *J. Biochem.*, 2000, **127**, 345-350.
31. Y. Fukuda, K. M. Tse, T. Nakane, T. Nakatsu, M. Suzuki, M. Sugahara, S. Inoue, T. Masuda, F. Yumoto, N. Matsugaki, E. Nango, K. Tono, Y. Joti, T. Kameshima, C. Song, T. Hatsui, M. Yabashi, O. Nureki, M. E. P. Murphy, T. Inoue, S. Iwata and E. Mizohata, Redox-coupled proton transfer mechanism in nitrite reductase revealed by femtosecond crystallography, *Proc. Natl. Acad. Sci. U.S.A.*, 2016, **113**, 2928-2933.
32. S. Horrell, S. V. Antonyuk, R. R. Eady, S. S. Hasnain, M. A. Hough and R. W. Strange, Serial crystallography captures enzyme catalysis in copper nitrite reductase at atomic resolution from one crystal, *IUCrJ*, 2016, **3**, 271-281.
33. M. Lintuluoto and J. M. Lintuluoto, Intra-electron transfer induced by protonation in copper-containing nitrite reductase, *Metallomics*, 2018, **10**, 565-578.
34. F. Jacobson, A. Pistorius, D. Farkas, W. De Grip, Ã. r. Hansson, L. SjÃ¶lin and R. Neutze, pH Dependence of Copper Geometry, Reduction Potential, and Nitrite Affinity in Nitrite Reductase, *J. Biol. Chem.*, 2007, **282**, 6347-6355.
35. D. Pinho, S. Besson, C. D. Brondino, B. de Castro and I. Moura, Copper-containing nitrite reductase from Pseudomonas chlororaphis DSM 50135, *Eur. J. Biochem.*, 2004, **271**, 2361-2369.
36. S. Ghosh, A. Dey, Y. Sun, C. P. Scholes and E. I. Solomon, Spectroscopic and computational studies of nitrite reductase: proton induced electron transfer and backbonding contributions to reactivity, *J. Am. Chem. Soc.*, 2009, **131**, 277-288.
37. E. J. Bedmar, E. F. Robles and M. J. Delgado, The complete denitrification pathway of the symbiotic, nitrogen-fixing bacterium Bradyrhizobium japonicum, *Biochemical Society Transactions*, 2005, **33**, 141-144.
38. M. J. Torres, M. I. Rubia, E. J. Bedmar and M. J. Delgado, Denitrification in Sinorhizobium meliloti, *Biochemical Society Transactions*, 2011, **39**, 1886-1889.
39. M. J. Barnett, R. F. Fisher, T. Jones, C. Komp, A. P. Abola, F. Barloy-Hubler, L. Bowser, D. Capela, F. Galibert, J. Gouzy, M. Gurjal, A. Hong, L. Huizar, R. W. Hyman, D. Kahn, M. L. Kahn, S. Kalman, D. H. Keating, C. Palm, M. C. Peck, R. Surzycki, D. H. Wells, K. C. Yeh, R. W. Davis, N. A. Federspiel and S. R. Long, Nucleotide sequence and predicted functions of the entire Sinorhizobium meliloti pSymA megaplasmid, *Proceedings of the National Academy of Sciences of the United States of America*, 2001, **98**, 9883-9888.
40. T. Kaneko, Y. Nakamura, S. Sato, K. Minamisawa, T. Uchiumi, S. Sasamoto, A. Watanabe, K. Idesawa, M. Iriguchi, K. Kawashima, M. Kohara, M. Matsumoto, S. Shimpo, H. Tsuruoka, T. Wada, M. Yamada and S. Tabata, Complete Genomic Sequence of Nitrogen-fixing Symbiotic Bacterium Bradyrhizobium japonicum USDA110, *DNA Research*, 2002, **9**, 189-197.
41. S. Mesa, J. d. D. Alché, E. Bedmar and M. J. Delgado, Expression of nir, nor and nos denitrification genes from Bradyrhizobium japonicum in soybean root nodules, *Physiologia Plantarum*, 2004, **120**, 205-211.

42. M. Bott, L. Thöny-Meyer, H. Loferer, S. Rossbach, R. E. Tully, D. Keister, C. A. Appleby and H. Hennecke, Bradyrhizobium japonicum cytochrome c550 is required for nitrate respiration but not for symbiotic nitrogen fixation, *Journal of bacteriology*, 1995, **177**, 2214.
43. J. C. Cristaldi, M. C. Gómez, P. J. González, F. M. Ferroni, S. D. Dalosto, A. C. Rizzi, M. G. Rivas and C. D. Brondino, Study of the Cys-His bridge electron transfer pathway in a copper-containing nitrite reductase by site-directed mutagenesis, spectroscopic, and computational methods, *Biochim. Biophys. Acta, Gen. Subj.*, 2018, **1862**, 752-760.
44. F. M. Ferroni, S. A. Guerrero, A. C. Rizzi and C. D. Brondino, Overexpression, purification, and biochemical and spectroscopic characterization of copper-containing nitrite reductase from Sinorhizobium meliloti 2011. Study of the interaction of the catalytic copper center with nitrite and NO, *J. Inorg. Biochem.*, 2012, **114**, 8-14.
45. F. Sanger, S. Nicklen and A. Coulson, DNA sequencing with chain termination method, *Proc. Natl. Acad. Sci. U.S.A.*, 1977, **74**, 5463-5467.
46. F. W. Studier, Stable expression clones and auto-induction for protein production in E. coli, *Methods Mol. Biol.*, 2014, **1091**, 17-32.
47. E. Arslan, H. Schulz, R. Zufferey, P. Künzler and L. Thöny-Meyer, Overproduction of the Bradyrhizobium japonicum c-Type Cytochrome Subunits of the cbb3 Oxidase in Escherichia coli, *Biochem. Biophys. Res. Commun.*, 1998, **251**, 744-747.
48. O. H. Lowry, N. J. Rosebrough, A. L. Farr and R. J. Randall, Protein measurement with the Folin phenol reagent, *J. Biol. Chem.*, 1951, **193**, 265-275.
49. U. K. Laemmli, Cleavage of structural proteins during the assembly of the head of bacteriophage T4, *Nature*, 1970, **227**, 680-685.
50. C. Coelho, P. J. González, J. G. Moura, I. Moura, J. Trincão and M. J. Romão, The crystal structure of Cupriavidus necator nitrate reductase in oxidized and partially reduced states, *J. Mol. Biol.*, 2011, **408**, 932-948.
51. L. Platts and R. J. Falconer, Controlling protein stability: Mechanisms revealed using formulations of arginine, glycine and guanidinium HCl with three globular proteins, *Int. J. Pharm.* , 2015, **486**, 131-135.
52. S. Stoll and A. Schweiger, EasySpin, a comprehensive software package for spectral simulation and analysis in EPR, *J. Magn. Reson.*, 2006, **178**, 42-55.
53. M. Biasini, S. Bienert, A. Waterhouse, K. Arnold, G. Studer, T. Schmidt, F. Kiefer, T. G. Cassarino, M. Bertoni, L. Bordoli and T. Schwede, SWISS-MODEL: modelling protein tertiary and quaternary structure using evolutionary information, *Nucleic Acids Res.*, 2014, **42**, W252-W258.
54. F. Kiefer, K. Arnold, M. Kunzli, L. Bordoli and T. Schwede, The SWISS-MODEL Repository and associated resources, *Nucleic Acids Res.*, 2009, **37**, D387-392.
55. K. Arnold, L. Bordoli, J. Kopp and T. Schwede, The SWISS-MODEL workspace: a web-based environment for protein structure homology modelling, *Bioinformatics*, 2006, **22**, 195-201.
56. N. Guex, M. C. Peitsch and T. Schwede, Automated comparative protein structure modeling with SWISS-MODEL and Swiss-PdbViewer: a historical perspective, *Electrophoresis*, 2009, **30 Suppl 1**, S162-173.

57. T. J. Dolinsky, J. E. Nielsen, J. A. McCammon and N. A. Baker, PDB2PQR: an automated pipeline for the setup of Poisson-Boltzmann electrostatics calculations, *Nucleic Acids Res.*, 2004, **32**, W665-667.
58. W. Humphrey, A. Dalke and K. Schulten, VMD: Visual molecular dynamics, *J. Mol. Graph.*, 1996, **14**, 33-38.
59. M. J. Frisch, G. W. Trucks, H. B. Schlegel, G. E. Scuseria, M. A. Robb, J. R. Cheeseman, G. Scalmani, V. Barone, B. Mennucci, G. A. Petersson, H. Nakatsuji, M. Caricato, X. Li, H. P. Hratchian, A. F. Izmaylov, J. Bloino, G. Zheng, J. L. Sonnenberg, M. Hada, M. Ehara, K. Toyota, R. Fukuda, J. Hasegawa, M. Ishida, T. Nakajima, Y. Honda, O. Kitao, H. Nakai, T. Vreven, J. Montgomery, J. A., J. E. Peralta, F. Ogliaro, M. Bearpark, J. J. Heyd, E. Brothers, K. N. Kudin, V. N. Staroverov, R. Kobayashi, J. Normand, K. Raghavachari, A. Rendell, J. C. Burant, S. S. Iyengar, J. Tomasi, M. Cossi, N. Rega, J. M. Millam, M. Klene, J. E. Knox, J. B. Cross, V. Bakken, C. Adamo, J. Jaramillo, R. Gomperts, R. E. Stratmann, O. Yazyev, A. J. Austin, R. Cammi, C. Pomelli, J. W. Ochterski, R. L. Martin, K. Morokuma, V. G. Zakrzewski, G. A. Voth, P. Salvador, J. J. Dannenberg, S. Dapprich, A. D. Daniels, O. Farkas, J. B. Foresman, J. V. Ortiz, J. Cioslowski and D. J. Fox, *Gaussian 09, Revision C.1. Gaussian, Inc., Wallingford CT*, 2009.
60. J.-D. Chai and M. Head-Gordon, Long-range corrected hybrid density functionals with damped atom-atom dispersion corrections, *Phys. Chem. Chem. Phys.*, 2008, **10**, 6615-6620.
61. W. D. Cornell, P. Cieplak, C. I. Bayly, I. R. Gould, K. M. Merz, D. M. Ferguson, D. C. Spellmeyer, T. Fox, J. W. Caldwell and P. A. Kollman, A Second Generation Force Field for the Simulation of Proteins, Nucleic Acids, and Organic Molecules, *J. Am. Chem. Soc.*, 1995, **117**, 5179-5197.
62. H. Zhang, M. J. Boulanger, A. G. Mauk and M. E. P. Murphy, Carbon Monoxide Binding to Copper-Containing Nitrite Reductase from Alcaligenes faecalis, *J. Phys. Chem. B* 2000, **104**, 10738-10742.
63. J. Heyd and G. E. Scuseria, Efficient hybrid density functional calculations in solids: Assessment of the Heyd–Scuseria–Ernzerhof screened Coulomb hybrid functional, *J. Chem. Phys.*, 2004, **121**, 1187-1192.
64. K. Olesen, A. Veselov, Y. Zhao, Y. Wang, B. Danner, C. P. Scholes and J. P. Shapleigh, Spectroscopic, Kinetic, and Electrochemical Characterization of Heterologously Expressed Wild-Type and Mutant Forms of Copper-Containing Nitrite Reductase from Rhodobacter sphaeroides 2.4.3†, *Biochemistry*, 1998, **37**, 6086-6094.
65. G. Denariaz, W. J. Payne and J. LeGall, The denitrifying nitrite reductase of Bacillus halodenitrificans, *Biochim. Biophys. Acta, Bioenerg.*, 1991, **1056**, 225-232.
66. Y. Fukuda, T. Tamada, H. Takami, S. Suzuki, T. Inoue and M. Nojiri, Cloning, expression, purification, crystallization and preliminary X-ray crystallographic study of GK0767, the copper-containing nitrite reductase from Geobacillus kaustophilus, *Acta Crystallogr. F*, 2011, **67**, 692-695.
67. Z. H. Abraham, D. Lowe and B. E. Smith, Purification and characterization of the dissimilatory nitrite reductase from Alcaligenes xylosoxidans subsp. xylosoxidans (NCIMB 11015): evidence for the presence of both type 1 and type 2 copper centres, *Biochem. J.*, 1993, **295**, 587-593.

68. H. J. Wijma, M. J. Boulanger, A. Molon, M. Fittipaldi, M. Huber, M. E. Murphy, M. P. Verbeet and G. W. Canters, Reconstitution of the type-1 active site of the H145G/A variants of nitrite reductase by ligand insertion, *Biochemistry*, 2003, **42**, 4075-4083.
69. S. Suzuki, K. Yamaguchi, K. Kataoka, K. Kobayashi, S. Tagawa, T. Kohzuma, S. Shidara and H. Iwasaki, Spectroscopic characterization and intramolecular electron transfer processes of native and type 2 Cu-depleted nitrite reductases, *J. Biol. Inorg. Chem.*, 1997, **2**, 265-274.
70. A. Veselov, K. Olesen, A. Sienkiewicz, J. P. Shapleigh and C. P. Scholes, Electronic Structural Information from Q-Band ENDOR on the Type 1 and Type 2 Copper Liganding Environment in Wild-Type and Mutant Forms of Copper-Containing Nitrite Reductase, *Biochemistry*, 1998, **37**, 6095-6105.
71. R. E. Tully, M. J. Sadowsky and D. L. Keister, Characterization of cytochromes c550 and c555 from Bradyrhizobium japonicum: cloning, mutagenesis, and sequencing of the c555 gene (cycC), *J. Bacteriol.*, 1991, **173**, 7887-7895.
72. G. W. Pettigrew, R. Gilmour, C. F. Goodhew, D. J. Hunter, B. Devreese, J. Van Beeumen, C. Costa, S. Prazeres, L. Krippahl, P. N. Palma, I. Moura and J. J. Moura, The surface-charge asymmetry and dimerisation of cytochrome c550 from Paracoccus denitrificans--implications for the interaction with cytochrome c peroxidase, *European journal of biochemistry*, 1998, **258**, 559-566.
73. M. R. Sawaya, D. W. Krogmann, A. Serag, K. K. Ho, T. O. Yeates and C. A. Kerfeld, Structures of Cytochrome c-549 and Cytochrome c6 from the Cyanobacterium Arthrospira maxima, *Biochemistry*, 2001, **40**, 9215-9225.
74. T. Gao and M. R. O'brian, Control of DegP-dependent degradation of c-type cytochromes by heme and the cytochrome c maturation system in Escherichia coli, *J. Bacteriol.*, 2007, **189**, 6253-6259.
75. F. Scholz, *Electroanalytical methods*, Springer, 2010.
76. K. Kataoka, K. Yamaguchi and S. Suzuki, Spectroscopic and electrochemical properties of cytochrome c 551 from Alcaligenes xylosoxidans GIFU 1051, *Bull. Chem. Soc. Jpn.*, 2000, **73**, 1839-1840.
77. C. Léger and P. Bertrand, Direct electrochemistry of redox enzymes as a tool for mechanistic studies, *Chem. Rev.*, 2008, **108**, 2379-2438.
78. V. Fourmond, T. Lautier, C. Baffert, F. Leroux, P. P. Liebgott, S. Dementin, M. Rousset, P. Arnoux, D. Pignol, I. Meynial-Salles, P. Soucaille, P. Bertrand and C. Léger, Correcting for electrocatalyst desorption and inactivation in chronoamperometry experiments, *Analytical chemistry*, 2009, **81**, 2962-2968.
79. M. J. Ellis, F. E. Dodd, G. Sawers, R. R. Eady and S. S. Hasnain, Atomic resolution structures of native copper nitrite reductase from Alcaligenes xylosoxidans and the active site mutant Asp92Glu, *J. Mol. Biol.*, 2003, **328**, 429-438.
80. L. B. LaCroix, S. E. Shadle, Y. Wang, B. A. Averill, B. Hedman, K. O. Hodgson and E. I. Solomon, Electronic structure of the perturbed blue copper site in nitrite reductase: spectroscopic properties, bonding, and implications for the entatic/rack state, *J. Am. Chem. Soc.*, 1996, **118**, 7755-7768.
81. M. A. Hough, R. R. Eady and S. S. Hasnain, Identification of the proton channel to the active site type 2 Cu center of nitrite reductase: structural and enzymatic properties of the His254Phe and Asn90Ser mutants, *Biochemistry*, 2008, **47**, 13547-13553.